Supplementary information for

CuSCN as a hole transport layer in inorganic solution-processed planar Sb_2S_3 solar cell: enabling carbon-based and semitransparent photovoltaics

Pankaj Kumar[1], Shujie You[1], Alberto Vomiero[1, 2]*

[1]Division of Materials Science, Department of Engineering Sciences and Mathematics, Luleå University of Technology, SE-971 87 Luleå, Sweden

[2]Department of Molecular Sciences and Nanosystems, Ca' Foscari University of Venice, Via Torino 155, 30172 Venezia Mestre, Italy

*Corresponding author

Email: alberto.vomiero@ltu.se

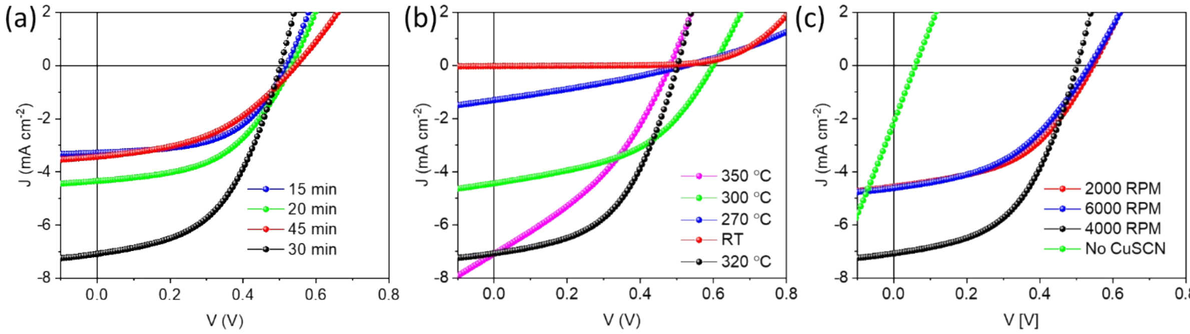

Figure S1. (a) The J-V curves of the best solar cells at different (a) Sb_2S_3 CBD times, (b) Sb_2S_3 annealing temperatures, and (c) CuSCN spin coating speeds.

Table S1. Photovoltaic parameters of the best solar cells with different CBD times.

CBD time [thickness][a]	J_{SC} [mA cm^{-2}]	V_{OC} [V]	FF [%]	PCE [%]
15 min [35 nm]	3.3	0.52	0.54	0.90
20 min [45 nm]	4.3	0.53	0.50	1.15
30 min [50 nm]	7.1	0.50	0.50	1.75
45 min [70 nm]	3.4	0.54	0.44	0.81

[a]Typical heights of the Sb_2S_3 islands.

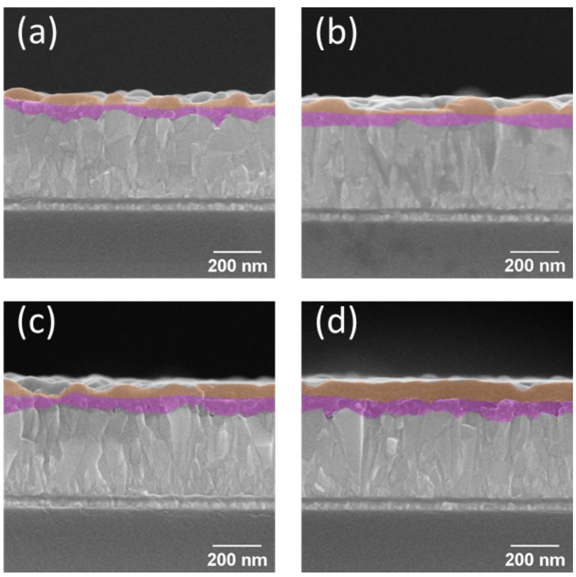

Figure S2. Cross-section images of FTO/TiO_2/CBD-Sb_2S_3 stack with different CBD times. (a) 15 min, (b) 20 min, (c) 30 min, and (d) 45 min. Island type growth can be clearly seen in (a) and (b).

Table S2. Photovoltaic parameters of the best solar cells with different annealing temperatures.

Annealing temperature	J_{SC} [mA cm^{-2}]	V_{OC} [V]	FF [%]	PCE [%]
RT	0.03	0.40	0.31	0.00
270 °C	1.3	0.53	0.29	0.20
300 °C	4.4	0.60	0.46	1.20
320 °C	7.1	0.50	0.50	1.75
350 °C	7.1	0.48	0.36	1.20

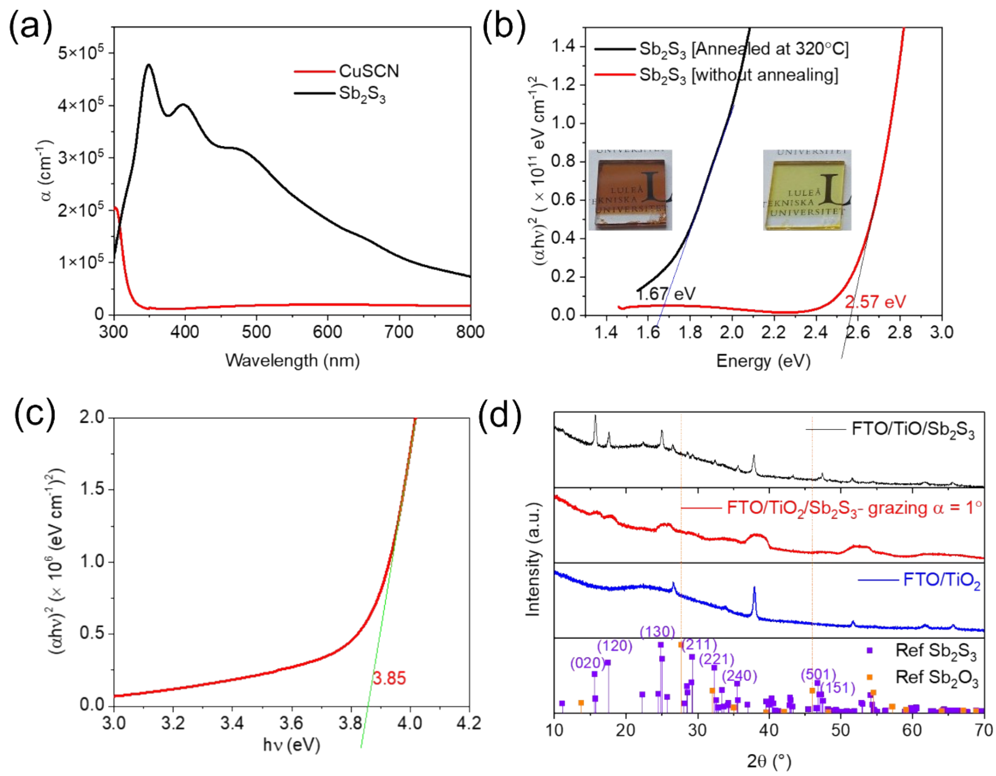

Figure S3. (a) Absorption spectra of CuSCN thin film on glass, Sb_2S_3, and Sb_2S_3 on FTO/TiO_2 substrates. Tauc-plots to calculate the bandgap of (b) Sb_2S_3 and (c) CuSCN thin films. (d) XRD spectrum of Sb_2S_3 thin film on FTO/TiO_2 substrates

Table S3. Photovoltaic parameters of the best solar cells with different RPMs of CuSCN deposition.

Spin coating RPM [thickness][a]	J_{SC} [mA cm^{-2}]	V_{OC} [V]	FF [%]	PCE [%]
2000 RPM [110 nm]	4.3	0.54	0.47	1.18
4000 RPM [70 nm]	7.1	0.50	0.50	1.75
6000 RPM [45 nm]	4.6	0.54	0.44	1.10
No CuSCN	2.6	0.05	0.23	0.03

[a] thickness measured from cross-section SEM images of FTO/CuSCN films.

Table S4. Electrical parameters of FTO, TiO_2, Sb_2S_3, and CuSCN, used in SCAPS-1D simulation.

Parameters	FTO[1,2]	TiO_2[3]	Sb_2S_3[3]	CuSCN
CBM (eV)	4.4	4.0	3.7	1.6[4]
Bandgap (eV)	3.5	3.3	1.7	3.8
Dielectric constant	9	31	7.1[5]	5.1[6]
CB N_{eff} (cm^{-3})	2.2×10^{18}	10^{19}	5×10^{19}	2.2×10^{18}[7]
VB N_{eff} (cm^{-3})	1.8×10^{19}	10^{19}	10^{20}	1.8×10^{18}[7]
$\mu_{electron}$ (cm^2/Vs)	20	10	0.8[3]	100[7]
μ_{hole} (cm^2/Vs)	10	1	0.2[3]	25[7]
Doping, $N_{A/D}$ (cm^{-3})	10^{19}	10^{17}	Intrinsic[3]	1.0×10^{18}[7]
Defect type[a]	-	Neutral	Neutral	
Defect density (cm^{-3})	-	10^{17}	10^{12}	10^{15}[8]

Defect capture cross-section (cm^{-2})	-	10^{-16} (n)	10^{-14} (n) 5×10^{-15} (p)	10^{-16} (p)
Defect energetic position (eV)	-	$E_v + 1.8$	$E_v + 0.52$	$E_v + 0.90$[9]
Thickness (nm)	50	50	50	50

[a]All the defect-related parameters were taken from Kondrotas et al.[3]
CBM: Conduction band maximum; CB/VB N_{eff}: conduction band/valence band effective density of states; μ: mobility

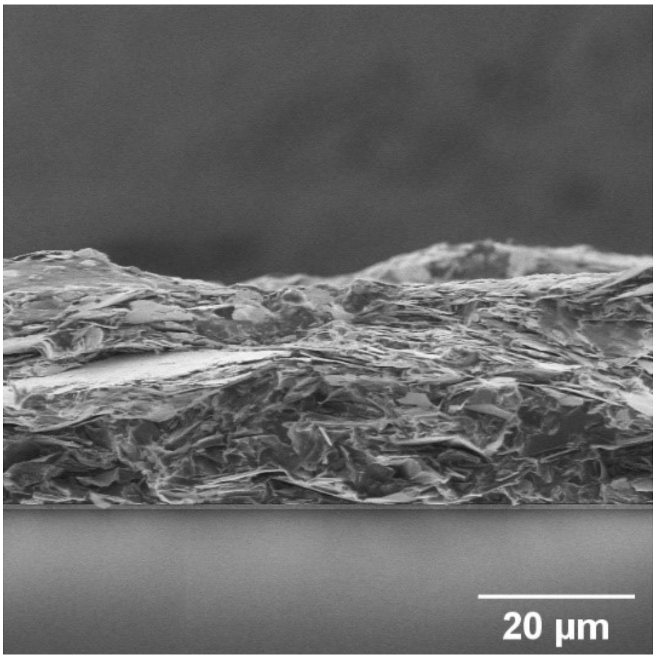

Figure S4. A zoomed-out SEM image of the C-electrode device.

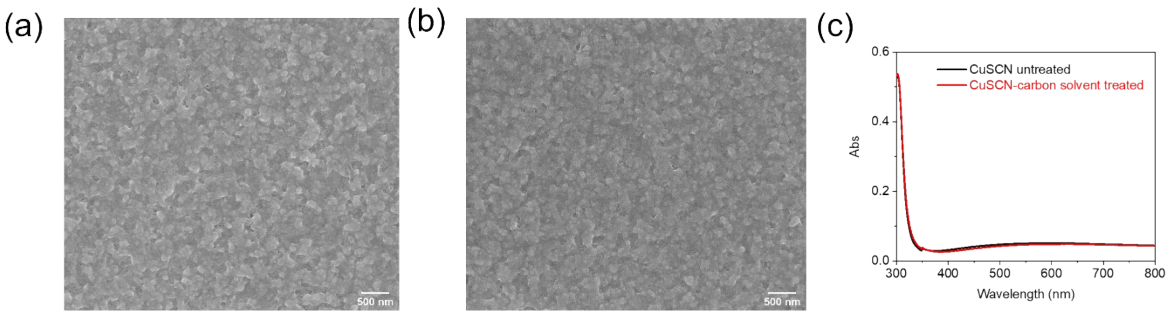

Figure S5. Top view SEM images of (a) FTO/TiO_2/Sb_2S_3/CuSCN and FTO/TiO_2/Sb_2S_3/CuSCN-carbon solvent treated films. (c) Absorption spectra of CuSCN films with and without treatment with carbon solvent.

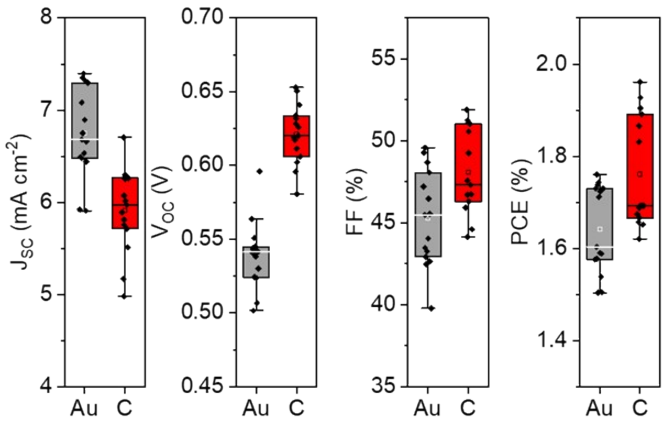

Figure S6: Statistical data of 15 devices fabricated using C and Au electrodes.

Table S5. Literature reports of planar solution processed Sb_2S_3 solar cells with CuSCN as HTL.

Electrode	CuSCN deposition	Sb_2S_3 deposition	V_{OC} [V]	J_{SC} [mA cm^{-2}]	FF [%]	PCE [%]	Ref
Au	Spin coating	CBD	0.46	5.44	0.33	0.80	[10]
Au	Spin coating	Thermal evaporation	0.60	6.43	0.44	1.69	[10]
Au	Impregnation	CBD	0.48	4.85	0.38	0.90	[11]
Au	Impregnation	Sputtering	0.59	5.26	0.54	1.67	[11]
Au	Wiping	CBD	0.55	4.30	0.35	0.83	[12]
Au	Spin coating	CBD	0.50	7.10	0.50	1.75	This work
Carbon			0.61	6.25	0.51	1.95	

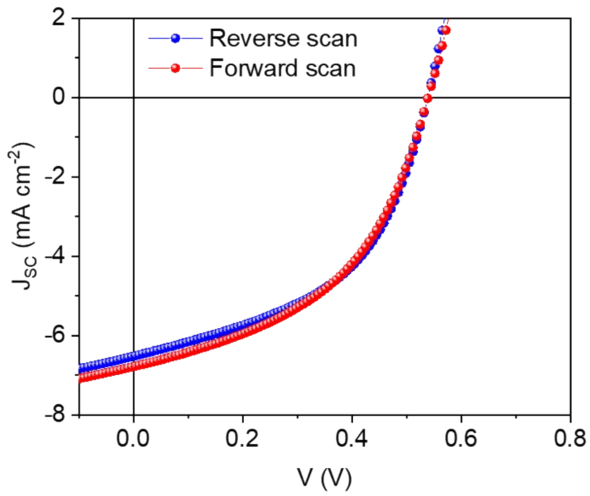

Figure S7. Forward vs. reverse scan of a device with Au electrode. Forward scan (-0.1 to 1 V): V_{OC} = 0.539, J_{SC} = 6.8 mA cm^2, FF = 0.46, PCE = 1.70 %; Reverse scan (1 to -0.1 V): V_{OC} = 0.538, J_{SC} = 6.5 mA cm^2, FF = 0.49, PCE = 1.70 %.

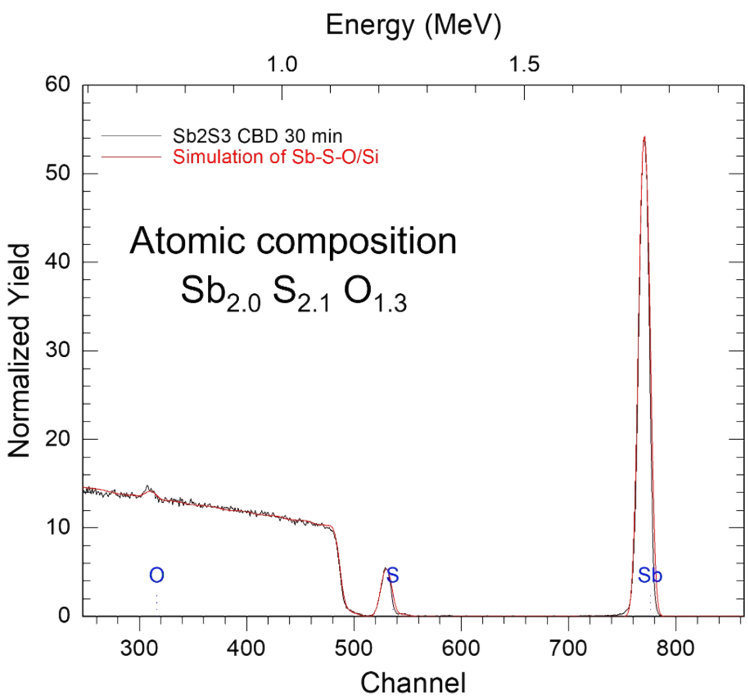

Figure S8. RBS spectrum of the annealed Sb_2S_3 film. Black line: experiment. Red line: RUMP code simulation. The atomic composition is obtained from the simulation.

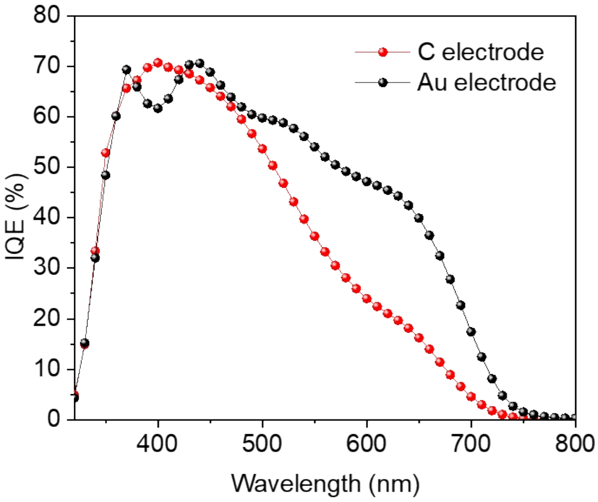

Figure S9. The internal quantum efficiency of champion solar cells with Au and C electrodes. IQE = EQE/(1-R_{device}), where R_{device} is the reflectance from the glass side which faces the sunlight.

Table S6. Parameters derived from EIS analysis of solar cells with varying top electrodes.

Electrode	$R_{s,EIS}$ [Ω]	R_{rec} or Rp [Ω]	CPE-T [F]	CPE-P	V_{bi} [V]	Defect density [cm^{-3}]
Carbon	198	45434	2.52×10^{-8}	0.95	1.45	6.75×10^{17}
Au	178	5261	5.93×10^{-8}	0.91	1.32	1.27×10^{18}

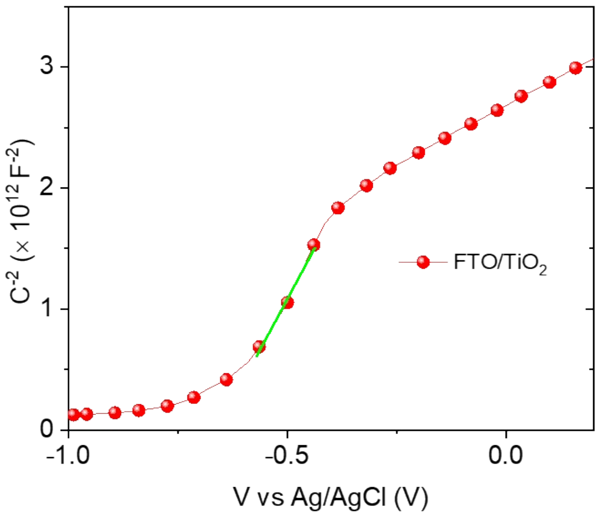

Figure S10. Mott-Schottky of FTO/TiO_2 thin film in 0.1 M Na_2SO_4 at 10 kHz. Ag/AgCl was used as a reference electrode. TiO_2 donor concentration (N_D) was calculated following previous reports.[13,14]

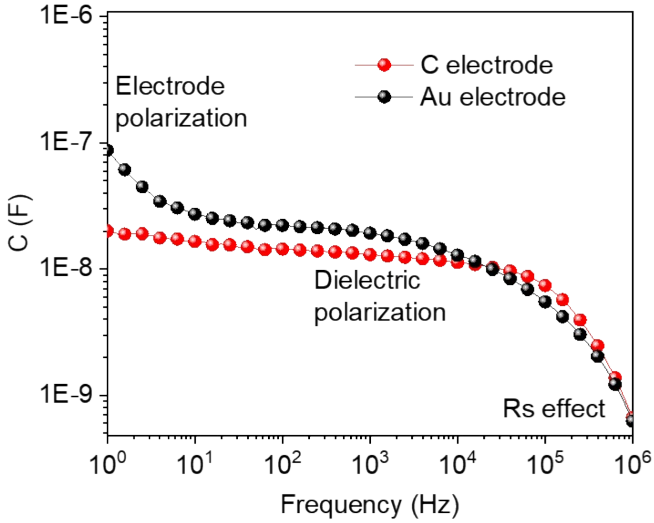

Figure S11. Capacitance vs. frequency curves for C and Au-based devices.

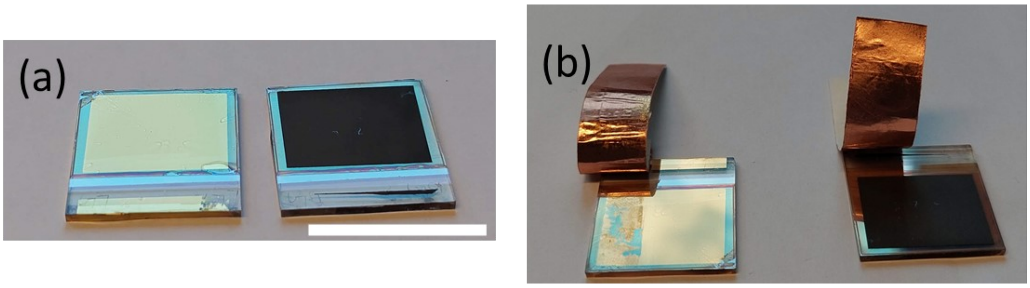

Figure S12. Adhesion test of Au and carbon-based devices. (a) before and (b) after peeling off with highly adhesive copper tape. Substrate size: 25 mm x 25 mm.

References:

1 S. Ahmed, F. Jannat, Md. A. K. Khan and M. A. Alim, *Optik*, 2021, **225**, 165765.
2 A. Kuddus, M. F. Rahman, S. Ahmmed, J. Hossain and A. B. M. Ismail, *Superlattices Microstruct.*, 2019, **132**, 106168.
3 R. Kondrotas, C. Chen and J. Tang, *Joule*, 2018, **2**, 857–878.
4 N. Wijeyasinghe, F. Eisner, L. Tsetseris, Y.-H. Lin, A. Seitkhan, J. Li, F. Yan, O. Solomeshch, N. Tessler, P. Patsalas and T. D. Anthopoulos, *Adv. Funct. Mater.*, 2018, **28**, 1802055.
5 M. T. Islam and A. K. Thakur, *Sol. Energy*, 2020, **202**, 304–315.
6 P. Pattanasattayavong, A. D. Mottram, F. Yan and T. D. Anthopoulos, *Adv. Funct. Mater.*, 2015, **25**, 6802–6813.
7 V. E. Madhavan, I. Zimmermann, A. A. B. Baloch, A. Manekkathodi, A. Belaidi, N. Tabet and M. K. Nazeeruddin, *ACS Appl. Energy Mater.*, 2020, **3**, 114–121.
8 A. Tara, V. Bharti, S. Sharma and R. Gupta, *Opt. Mater.*, 2021, **119**, 111362.
9 J. E. Jaffe, T. C. Kaspar, T. C. Droubay, T. Varga, M. E. Bowden and G. J. Exarhos, *J. Phys. Chem. C*, 2010, **114**, 9111–9117.
10 Y. O. Mayon, T. P. White, R. Wang, Z. Yang and K. R. Catchpole, *Phys. Status Solidi A*, 2016, **213**, 108–113.
11 X. Zhang, S. Yoshioka, N. Loew and M. Ihara, *ECS Trans.*, 2014, **64**, 1.
12 T. Muto, G. Larramona and G. Dennler, *Appl. Phys. Express*, 2013, **6**, 072301.
13 R. van de Krol, A. Goossens and J. Schoonman, *J. Electrochem. Soc.*, 1997, **144**, 1723.
14 E.-J. Lee and S.-I. Pyun, *J. Appl. Electrochem.*, 1992, **22**, 156–160.